# Simultaneous Detection of Multiple Biomarkers with over Three Orders of Concentration Difference Using Phase Change Nanoparticles

**ARTICLE** *in* ANALYTICAL CHEMISTRY · FEBRUARY 2011

Impact Factor: 5.64 · DOI: 10.1021/ac103102h · Source: PubMed



**4 AUTHORS**, INCLUDING:

Chaoming Wang
Southwest Jiaotong University
**36** PUBLICATIONS **233** CITATIONS

SEE PROFILE

Zhaoyong Sun
Binghamton University
**27** PUBLICATIONS **463** CITATIONS

SEE PROFILE

analytical chemistry

ARTICLE

pubs.acs.org/ac

# Simultaneous Detection of Multiple Biomarkers with over Three Orders of Concentration Difference Using Phase Change Nanoparticles

Chaoming Wang,[†,‡] Zhaoyong Sun,[†] Liyuan Ma,[†] and Ming Su*[,†,‡,§]

[†]NanoScience Technology Center, [‡]Department of Mechanical, Materials, and Aerospace Engineering, [§]School of Electrical Engineering and Computer Science, University of Central Florida, Orlando, Florida 32826, United States

Supporting Information

**ABSTRACT:** A big challenge for multiplexed detection of cancer biomarkers is that biomarker concentrations in body fluid differs several orders of magnitude. Existing techniques are not suitable to detect low- and high-concentration biomarkers (protein and DNA) at the same time, and liquid chromatography or electrophoresis is used to separate or purify target biomarkers before analysis. This paper describes a new broad-range biomarker assay using solid to liquid phase change nanoparticles, where a panel of metallic nanoparticles (i.e., metals and eutectic alloys) are modified with a panel of ligands to establish a one-to-one correspondence and attached onto ligand-modified substrates by forming sandwiched complexes. The melting peak and fusion enthalpy of phase change nanoparticles during thermal analysis reflect the type and concentration of biomarkers, respectively. The thermal readout condition can be adjusted in such a way that multiple biomarkers with concentration difference over 3 orders of magnitude have been simultaneously detected under the same condition.

Although many cancer biomarkers have been discovered, it is clear that no single biomarker can be used to detect lethal cancers from indolent ones.[1−4] The wide use of prostate specific antigen (PSA) screening has led to overdiagnosis and treatment of more than 1 million men in the United States. Parallel to the effort of finding more specific biomarkers, one feasible way of providing better predictive values is to detect multiple cancer biomarkers with low specificity simutaneously.[5−10] However, a great challenge of existing techniques for multiple biomarker detection is that concentrations of cancer biomarker differ several (eight to nine) orders of magnitude from pg/mL up to mg/mL, where a large proportion of biomarkers appear in the low concentration range.[11−13] However, at conditions that low concentration ones can be detected, signals from high concentration ones are saturated for techniques such as DNA microarray, enzyme-linked immunosorbent assay (ELISA), polymerase chain reaction (PCR), and nanoparticle-based detection.[14−20] Briefly, a DNA microarray has identical features, binding capacity, and a narrow range of detection concentration.[21−23] The signal−target ratio in ELISA depends on conjugation of the fluorescence label on each antibody, is constant after surface modification, and cannot adjust the concentration range of detection.[24,25] PCR provides saturated signals at high biomarker or enzyme concentration.[26,27] Most of these techniques do not have high multiplicity, and biomarkers of different types such as DNAs and proteins cannot be detected simultaneously at the same condition. As a result, liquid chromatography or electrophoresis has to be used to separate biomarkers prior to analysis.

This paper describes a new biosensing method based on solid−liquid phase change nanoparticles, where each type of nanoparticles is conjugated with ligands of according protein and DNA biomarkers and then immobilized on ligand-modified substrates by forming a double helix DNA chain or sandwiched antibody−antigen complex. The type and concentration of biomarkers are reflected in melting temperature and fusion enthalpy of nanoparticles in differential scanning calorimetry (DSC). The characters of nanoparticles such as nanoparticle size, materials, grafting density, and readout condition (i.e., thermal ramp rate) can be adjusted so that multiple biomarkers with concentration difference of over 3 orders of magnitude can be detected at the same time and under the same condition (Scheme 1). It is anticipated that the concentration range can be extended to 6−11 orders of magnitude by optimizing detection conditions.

## MATERIALS AND METHOD

**Materials and Chemicals.** Oligonucleotides are customer-synthesized at Integrated DNA Technologies, Inc. (Coralville, IA) with desired sequences. Capture single stranded DNA: ssDNA1 (5′-/5AmMC6/ATTATTATTATGTGGTTGCTGTGT-3′), ssDNA2 (5′-5AmMC6/ATTATTAAGCGTGTACTGAACT-3′); target ssDNA1 (3′-TACACCAACGACACAA ATGTTATTAGG-5′), ssDNA2 (3′-TCGCACATGACTTGAAATGTTATTAGG-5′); probe ssDNA1 (5′-TTAC AATAATCCATTATTATTA/3ThioMC3-D-3′), ssDNA2 (5′-TTACAATAATCCATTAT-TATTA/3Thio-MC3-D-3′). Human IgG and its antibody and prostate specific antigen (PSA) are obtained from Sigma. Two types of mouse antihuman PSA monoclonal antibodies (CHYH1 and CHYH2) are obtained from Anogen/Yes Biotech Laboratory. Organometallic precursors such as indium acetate, lead acetate, bismuth acetate, tin acetate, and polyvinylpyrrolidone

**Received:** November 24, 2010
**Accepted:** January 27, 2011
**Published:** February 21, 2011

  

(PVP, molecular weight of 11000) and ethylene glycol are from Aldrich. Disuccinimidyl suberate (DSS), N-succinimidyl(4-iodoacetyl)aminobenzoate (SIAB), as well as tris(2-carboxyethyl) phosphine (TCEP) are obtained from Thermo Fisher Scientific (Rockford, IL). Anhydrous dimethyl sulfoxide (DMSO), *n*-propyltriethoxysilane, and 3-aminopropyltriethoxysilane (APTES) are obtained from VWR (West Chester, PA). Phosphate buffer saline, bovine serum albumin (BSA), and Tween-20 are obtained from Sigma. All immuno-reagents are dissolved in pH 7.4 phosphate saline (PBS) buffer (0.01 M in phosphate, 0.14 M NaCl, 2.7 mM KCl) unless otherwise noted. Ultrapure water is used throughout experiment.

**Nanoparticle Synthesis and Characterization.** The phase change nanoparticles of metals and alloys have been synthesized by thermal decompositions of organometallic precursors (indium acetate, lead acetate, tin acetate, or bismuth acetate) with stoichiometric ratios.[28] In brief, the precursors and polyvinylpyrrolidone (molecular weight of 11000) are dissolved in ethylene glycol and stirred for 10 min to make a homogeneous solution. After the mixture is refluxed at 200 °C for 20 min to decompose precursors under nitrogen protection, the product is quenched by pouring the mixture in ethanol precooled at 0 °C. The as-prepared nanoparticles are then centrifuged at 3000 rpm for 10 min. After removing the supernatant, the nanoparticles are washed by ethanol three times. A droplet of nanoparticles in ethanol solution is deposited onto a carbon grid. After solvent evaporation, a JEOL 1011 transmission electron microscope (TEM) operated at 100 kV is used to determine the size and shape of the nanoparticles. A Zeiss Ultra 55 scanning electron microscope (SEM) at accelerating voltage of 10 kV is used to derive morphology and size distribution of nanoparticles. The compositions of nanoparticles are analyzed by using an energy dispersive X-ray (EDX) detector. A differential scanning calorimetry (PerkinElmer DSC7) is used to study thermophysical behaviors of nanoparticles. An Olympus BX51 M fluorescence microscopy is used to measure the fluorescence of fluorescein isothiocyanate-labeled bovine serum albumin (FITC-BSA) immobilized on thin films.

**Surface Modification.** The surface oxidized nanoparticles are modified with amine-functionalized monolayers by reacting with 3-aminopropyltriethoxysilane (APTES). In order to control ligand grafting density, a monofunctional silane (i.e., *n*-propyltriethoxysilane) is used to comodify nanoparticles at a variety of molar ratios (1:0, 1:1, 1:2, 1:5, and 1:10). The modification is performed by immersing nanoparticles in toluene that contains 5% (v/v) of the mixture of silane at a certain ratio. After reacting for 1 h at room temperature, nanoparticles are washed with toluene and dimethyl sulfoxide (DMSO) three times to remove excess silane. To conjugate single stranded DNA (ssDNA) onto nanoparticles, the amine groups at nanoparticles are activated with 1 mM N-succinimidyl(4-iodoacetyl)aminobenzoate (SIAB) in DMSO for 1 h. The disulfide-containing probe ssDNA is reduced with 0.25 M tris(2-carboxyethyl) phosphine (TCEP) at pH 4.5 in tris(hydroxymethyl)aminomethane (TE) buffer at 37 °C for 10 min. After removing excess SIAB by centrifugation, nanoparticles are incubated with 20 $\mu$M 3′ thiolated probe ssDNA in a phosphate buffer (PBS, pH 8.0) at room temperature. In order to conjugate protein, amine-modified nanoparticles are activated by incubating with a 1 mM DSS (disuccinimidyl suberate) cross-linker dissolved in DMSO for 1 h, which is followed by incubating with an antibody in PBS for 3 h. In order to immobilize ligands on an aluminum pan for DSC readout, the native oxide on aluminum is modified to have amine functional groups by vapor deposition of APTES at 100 °C for 1 h. The surface is washed by DMSO and then immersed in DMSO containing DSS (1 mM) for 1 h. After washing with DMSO and PBS three times, the aluminum surface is incubated with amine-functionalized capture ssDNA in PBS or a mixture of capture ssDNA and antibodies in 4X saline sodium citrate (SSC) buffer for 2 h. Unreacted ssDNAs or proteins are removed by washing thoroughly with a buffer solution that contains 1%(w/v) BSA and 0.05% Tween-20.

**Biomarker Detection.** Antibody or ssDNA modified aluminum pans are incubated with target ssDNA or protein (antigen) at various concentrations inside a buffer solution at room temperature for 3 h. After washing with PBS or SSC buffer, the aluminum pan with immobilized ssDNA or proteins is immersed in a buffer (PBS or SSC) that contains ssDNA or antibody-modified nanoparticles for 1 h. The substrate is rinsed thoroughly with a buffer and dried for thermal readout. A PerkinElmer DSC (DSC7) is used to determine the melting point and fusion enthalpy of immobilized nanoparticles at a certain ramp rate, where an empty aluminum pan is used as reference to derive the difference in heat flow of the sample and reference. The nature and concentration of biomarkers can be derived from the melting point and heat flow of nanoparticles on the basis of one-to-one correspondence between nanoparticles and the biomarker. The DSC baselines are flattened using Origin software to remove the slope and noise after collection.

## RESULTS AND DISCUSSION

The multiplicity of thermal detection depends on peak width, thermal scan range, and type of nanoparticles. In the temperature range of 100−1000 °C, although the available number of metals is limited, the number of eutectic alloys with a sharp melting peak is large and can be identified from the phase diagram. The peak width depends on the heat transfer rate, thermal conductivity of the atmosphere, and thermal ramp rate and could be derived from Gray's model based on energy conservation and Newton's law.[29] The melting peak shape for a small amount of sample has been shown to consist of two half-peaks: the first half-peak has a straight line slope, and the second half-peak shows an exponential decay. The width of the melting peak can be derived from a modified equation

$$w = 0.5\beta \times \Delta t = 0.5\beta \times (t_1 + t_2)$$
$$= 0.5\beta \times \left[ RC_s \left( \sqrt{1 + \frac{2\Delta H}{RC_s{}^2\beta}} - 1 \right) + RC_s \ln(100) \right] \quad (1)$$

where $R$ is thermal resistance, $C_s$ is the total sample heat capacity, $\Delta H$ is the latent heat of fusion, $\beta$ is the heating rate; $t_1$ and $t_2$ are the times needed for the solid to melt and the temperature to catch up with programmed temperature, respectively. Theoretically, $t_2$ is infinitely long, but for practical purposes, $t_2$ is defined as the time for the heat flow to fall below 1% of its maximum. The sensitivity and concentration range of detection can be adjusted by changing materials, particle size, and operating conditions (ramp rate). Assuming that nanoparticles have a uniform radius ($r$), and the grafting density of ligands on nanoparticles is $\alpha$, the number of

biomarkers ($n$) that can be detected will be

$$n = \frac{3Q\alpha}{4\pi r^3 \rho \times \beta \times \Delta H} \quad (2)$$

where $Q$ is detectable heat flow (determined by instrument), and $\rho$ is density of nanoparticle.

Indium, lead−tin alloy, tin and bismuth nanoparticles (melting temperatures of 156, 183, 231, and 271 °C, respectively) have uniform sizse at 30, 100, 100, and 200 nm (Figure 1A−D), respectively. The as-made nanoparticles are surface oxidized by heating in air at 70 °C for 30 min. The formation of oxide shells around metallic nanoparticles is confirmed by X-ray photoelectron spectroscopy (XPS). Two asymmetrical peaks observed at 159 and 164.4 eV, as shown in panel (E) of Figure 1, correspond to Bi $4f_{7/2}$ and Bi $4f_{5/2}$ of bismuth oxide, which reflect formation of oxide at nanoparticles. After sputtering nanoparticles with argon ion for 10 s at 3 kV and 14 $\mu$A, two peaks which are $4f_{7/2}$ and $4f_{5/2}$ peaks of bismuth metal, appear at 156.9 and 162.2 eV (Figure 1F).[30,31] Similar oxide core−metal shell structures have also been found in other three types of nanoparticles.

Panel (A) of Figure 3 shows a ramp rate-dependent peak width for different nanoparticles, where half widths at maximum height (HWMH) of nanoparticles increase as ramp rate increases from 1 to 50 °C/min. The existence of melting peaks confirms that metallic nanoparticles preserve in oxide shells. In the case of tin nanoparticles, the peak width changes from 1.5 to 14 °C when ramp rate increases from 1 to 50 °C/min. By fitting data with eq 1, the thermal resistance and total sample heat capacity are determined to be $5.0 \times 10^{-3}$ °C/mW and 33.8 mJ/°C, respectively. On the other hand, the contribution of nanoparticles on melting time can be derived from

$$\frac{(T_s - T_m) \times \tau}{\left(\frac{\rho_l Q_l}{k_l}\right)} = r_p^2 \left[\frac{1}{3}\left(\frac{r}{r_p}\right)^3 - \frac{1}{2}\left(\frac{r}{r_p}\right)^2 + \frac{1}{6}\right] \quad (3)$$

where $T_s$ and $T_m$ are surface temperature and melting point of nanoparticles, respectively; $\tau$ is the melting time when the radius of solid is $r$; $r_p$ is the radius of nanoparticles; $Q_l$ is the latent heat of fusion of nanoparticles; $k_l$ is the thermal conductivity of nanoparticles; and $\rho_l$ is the density of nanoparticles. For indium nanoparticles, $k_{In}$ is 81.8 W m$^{-1}$ K$^{-1}$, $r_{In}$ is 50 nm, $Q_{In}$ is 28.52 kJ/kg, and $\rho_{In}$ is 7310 kg/m$^3$. Replacing all symbols with numbers and letting $r$ equal 0 nm, eq 3 is rewritten as $\tau(T_s - T_m) = 1.1 \times 10^{-9}$s K. Assuming $T_s - T_m = 0.1$ K, $\tau$ is 11 ns. A linear relation exists between the melting time and $1/(T_s - T_m)$ as shown in panel (B) of Figure 2 for four types of nanoparticles. The difference in peak width induced by the melting time difference is less than 0.01 °C. The small contribution on peak width suggests that heat transfer inside nanoparticles is not important on peak width; instead, the heat transfer from heater through air to aluminum pan and nanoparticles is important. Panel (C) of Figure 2 shows melting curves of indium nanoparticles at ramp rates of 1, 2, 5, 10, 20, and 50 °C/min. The similarity among peaks suggests surface oxidation is not incremental after reaching equilibrium. The peak shifts to high temperature as the ramp rate increases. The peak area is linearly proportional to the heating rate in the range from 1 to 500 °C/min (Figure 2D). Providing the equipment sensitivity depends on rms (root-mean-square) noise; the large heat flow means that detectable limits can be lowered by 500 times.

The ligand grafting density around nanoparticles affects the detection range and sensitivity. The grafting density of silane on each type of material is first derived from fluorescence intensity after cross-linking fluorescence-labeled bovine serum albumin at amine-terminated thin films evaporated onto silicon substrates. The different metallic/alloy thin films with a thickness of 100 nm are produced on the silicon substrates by thermally deposited corresponding metallic/alloy powder. From relative intensities of

**Scheme 1. Simultaneous Detection of Multiple Biomarkers Using Phase Change Nanoparticles**

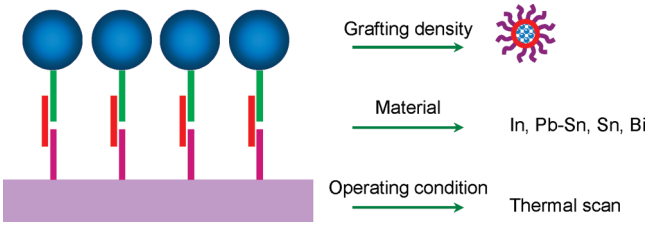


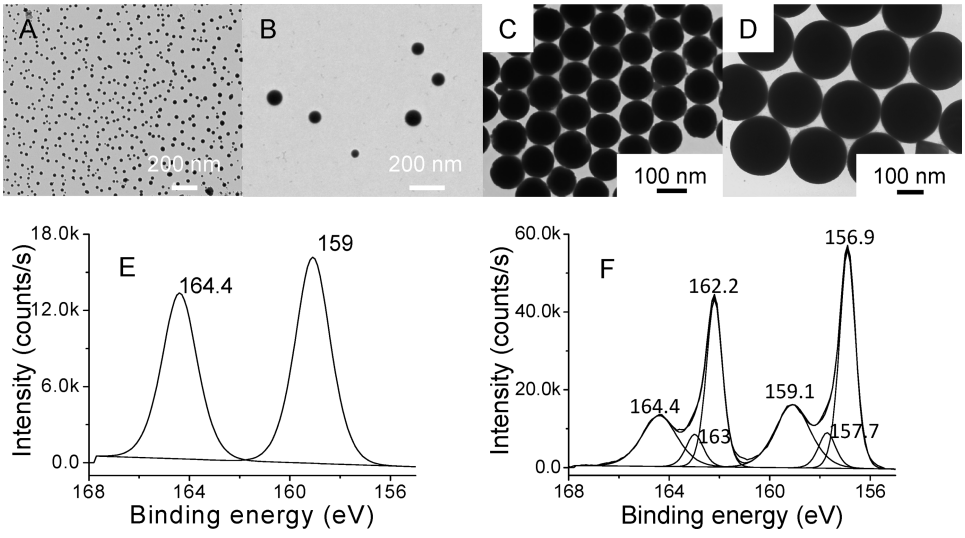


**Figure 1.** TEM images of indium (A), lead−tin alloy (B), tin (C) and bismuth (D) nanoparticles. XPS spectra of bismuth nanoparticles before (E) and after (F) sputtering with argon ions.


dx.doi.org/10.1021/ac103102h |*Anal. Chem.* 2011, 83, 2215–2219

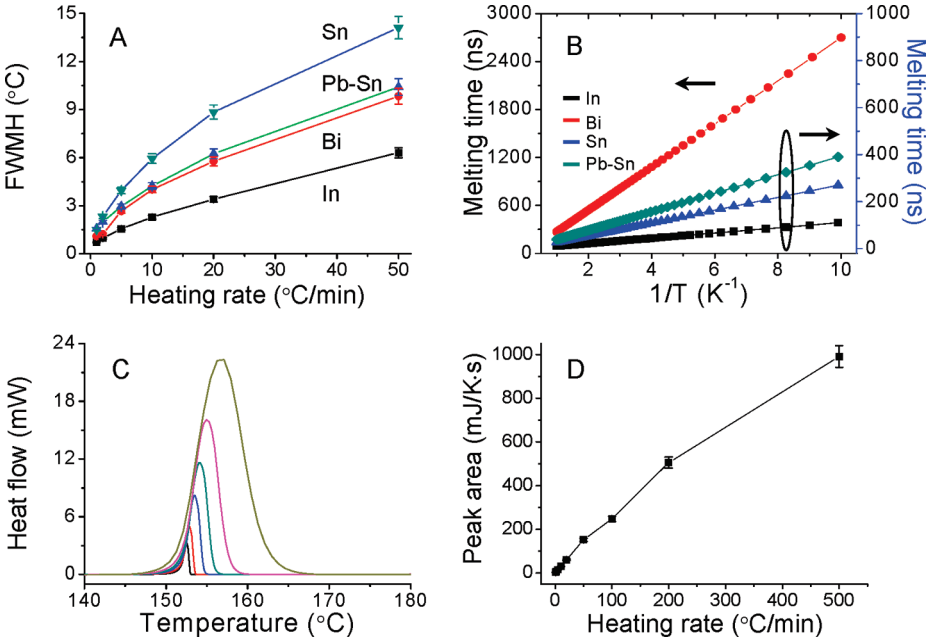


**Figure 2.** Ramp rate-dependent peak width for indium, bismuth, tin, and lead−tin nanoparticles (A); melting time of 100 nm indium, lead−tin, tin, and bismuth nanoparticles (B); DSC curves of 5 mg of indium nanoparticles at ramp rates of 1, 2, 5, 10, 20, and 50 °C/min (C); ramp rate dependent peak area (D).

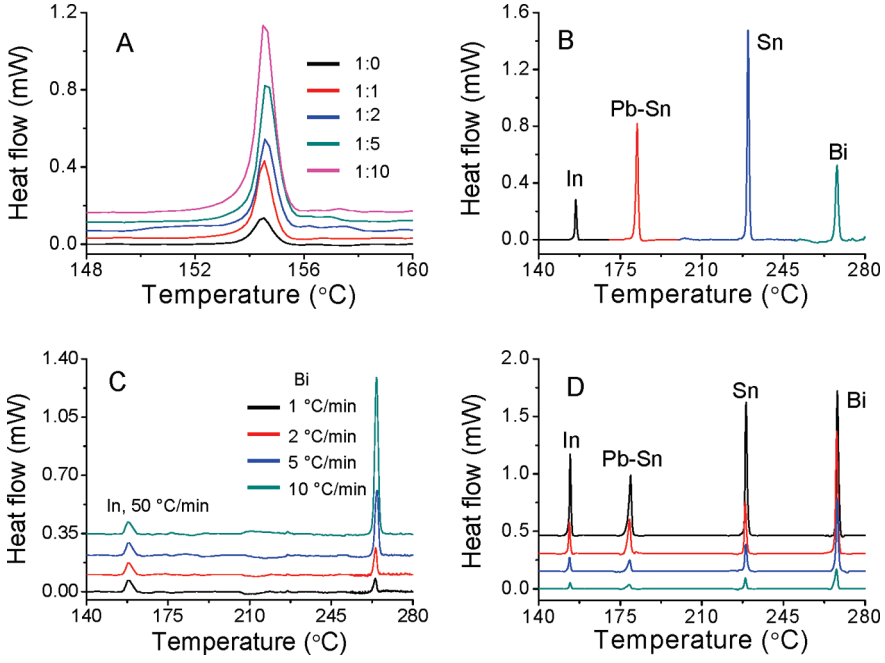


**Figure 3.** DSC curves of indium nanoparticles after detecting 10 nM ssDNA1 at different ratios of APTES and *n*-propyltriethoxysilane (1:0, 1:1, 1:2, 1:5, and 1:10) (A); DSC curves of indium, bismuth, tin, and lead−tin alloy nanoparticles after detecting ssDNA1 at concentrations of 10 nM (B); DSC curves of indium nanoparticles after detecting 100 pM ssDNA1 at a ramp rate of 50 °C/min and bismuth nanoparticles after detecting 100 nM ssDNA2 at a different ramp rate (1, 2, 5, and 10 °C/min) (C); DSC curves of indium, lead−tin, tin, and bismuth nanoparticles after detecting ssDNA1(100nM, 10 nM, 1 nM, and 100 pM), target ssDNA2(100nM, 10 nM, 1 nM, and 100 pM), PSA(100, 20, 10, and 5 pg/mL), and human IgG (10, 2, 1, and 0.5 ng/mL), respectively.

fluorescence images (Figure 1 of the Supporting Information), the ratio of ligand grafting densities of silane on indium, lead−tin alloy, tin, and bismuth thin films are determined as 1:1:2:2. Panel (A) of Figure 3 shows grafting density-dependent melting of immobilized nanoparticles, where melting curves from top to bottom correspond to 10 nM ssDNA1, respectively. Changing the molar ratio from 1:0 to 1:10 leads to larger melting peaks, which is consistent with eq 2, where the peak area is larger at lower grafting density providing others are the same. Heat flow can be changed using materials with different latent heats. The latent heats for indium, lead, tin, and bismuth are 28.5, 23, 58.5, and 52 J/g, respectively, and that for the lead−tin alloy

($Pb_{37}Sn_{63}$) is 45.4 J/g, which is derived by taking the mass fraction ($x$) into consideration using $H = xH_a + (1 - x)H_b$, and $H_a$ and $H_b$ are latent heats of metals. Panel (B) of Figure 3 shows DSC curves of four types of nanoparticles immobilized on aluminum plates after detecting 10 nM target ssDNA1. The peak area of immobilized tin nanoparticles is the largest because the latent heat of tin (58.5 J/g) is larger than other type nanoparticles.

The thermal scan can be programmed with multiple ramp rates. Panel (C) of Figure 3 shows four DSC curves of indium and bismuth nanoparticles, where melting peaks of indium nanoparticles are collected after detecting 100 pM ssDNA1 at 50 °C/min; the melting peaks of bismuth nanoparticles are collected after detecting 100 nM ssDNA2 at variable ramp rates from 1 to 10 °C/min. A discontinuity in heat flow induced by a ramp rate change at 200 °C is removed for display purpose. The variable rate scan is important for several reasons: (1) Overlapped peaks can be separated from each other. (2) Peak area (heat flow and sensitivity) can be varied. (3) Analysis time can be reduced by quickly scanning between peaks. These nanoparticles are used to detect four types of biomarkers (two types of DNA and two types of protein) in the same SSC buffer. Panel (D) of Figure 3 shows four DSC curves, where each of curve contains four types of nanoparticles immobilized on aluminum. Indium nanoparticles are used to detect ssDNA1 (100 nM to 100 pM). Lead−tin nanoparticles are used to detect ssDNA2 (100 nM to 100 pM). Tin nanoparticles are used to detect PSA (100 to 5 pg/mL). Bismuth nanoparticles are used to detect human IgG (10 to 0.5 ng/mL).

The concentration detection range can be estimated using the following parameters. DSC allows the ramp rate to be adjusted in the range of 0.02−500 °C/min, meaning that the detectable heat flow (concentration range) can be adjusted over 4 orders of magnitude. The diameter of nanoparticles can be changed from 30 to 200 nm. The grafting sites on nanoparticles can be any number from one to $4\pi \times 1000$.[32] The latent heat of fusion can be changed from 23 J/g for indium to 205 J/g for copper. According to eq 2, the upper limit of concentration will be $2.5 \times 10^{14}$ and the lower limit of concentration will be $1.6 \times 10^{3}$; thus, the concentration range is derived as 11 orders of magnitude. This method has been used successfully in detecting two DNA biomarkers whose concentrations are at 100 nM and 100 pM, spanning 3 orders of magnitude (Figure 3C).

## ■ ASSOCIATED CONTENT

**Supporting Information.** Additional information as noted in text. This material is available free of charge via the Internet at http://pubs.acs.org.

## ■ AUTHOR INFORMATION

**Corresponding Author**
*E-mail: mingsu@mail.ucf.edu.

## ■ ACKNOWLEDGMENT

This project was supported by the National Science Foundation, Florida Department of Health, and Department of Defense.

## ■ REFERENCES

(1) Ransohoff, D. F. *Science* **2003**, *299*, 1679–1680.
(2) Hinestrosa, M. C.; Dickersin, K.; Klein, P.; Mayer, M.; Noss, K.; Slamon, D.; Sledge, G.; Visco, F. M. *Nature Rev. Cancer* **2007**, *7*, 309–315.
(3) Cagir, B.; Gelmann, A.; Park, J.; Fava, T.; Tankelevitch, A.; Bittner, E. W.; Weaver, E. J.; Palazzo, J. P.; Weinberg, D.; Fry, R. D.; Waldman, S. A. *Ann. Intern. Med.* **1999**, *131*, 805–812.
(4) Kozak, K. R.; Su, F.; Whitelegge, J. P.; Faull, K.; Reddy, S.; Farias-Eisner, R. *Proteomics* **2005**, *5*, 4589–4596.
(5) Makarov, D. V.; Loeb, S.; Getzenberg, R. H.; Partin, A. W. *Annu. Rev. Med.* **2009**, *60*, 139–151.
(6) Rhodes, D. R.; Sanda, M. G.; Otte, A. P.; Chinnaiyan, A. M.; Rubin, M. A. *J. Natl. Cancer Inst.* **2003**, *95*, 661–668.
(7) Smith, M. Q.; Staley, C. A.; Kooby, D. A.; Styblo, T.; Wood, W. C.; Yang, L. *Curr. Mol. Med.* **2009**, *9*, 1017–1023.
(8) Michalet, X.; Pinaud, F. F.; Bentolila, L. A.; Tsay, J. M.; Doose, S.; Li, J. J.; Sundaresan, G.; Wu, A. M.; Gambhir, S. S.; Weiss, S. *Science* **2005**, *307*, 538–544.
(9) Medintz, I. L.; Uyeda, H. T.; Goldman, E. R.; Mattoussi, H. *Nat. Mater.* **2005**, *4*, 435–446.
(10) Jaiswal, J. K.; Mattoussi, H.; Mauro, J. M.; Simon, S. M. *Nat. Biotechnol.* **2003**, *21*, 47–51.
(11) Etzioni, R.; Urban, N.; Ramsey, S.; McIntosh, M.; Schwartz, S.; Reid, B.; Radich, J.; Anderson, G.; Hartwell, L. *Nature Rev. Cancer* **2003**, *3*, 243–252.
(12) Fan, R.; Vermesh, O.; Srivastava, A.; Yen, B. K. H.; Qin, L.; Ahmad, H.; Kwong, G. A.; Liu, C.-C.; Gould, J.; Hood, L.; Heath, J. R. *Nat. Biotechnol.* **2008**, *26*, 1373–1378.
(13) Nagrath, S.; Sequist, L. V.; Maheswaran, S.; Bell, D. W.; Irimia, D.; Ulkus, L.; Smith, M. R.; Kwak, E. L.; Digumarthy, S.; Muzikansky, A.; Ryan, P.; Balis, U. J.; Tompkins, R. G.; Haber, D. A.; Toner, M. *Nature* **2007**, *450*, 1235–1239.
(14) Guo, Q. M. *Curr. Opin. Oncol.* **2003**, *15*, 36–43.
(15) Hoshi, S.; Kobayashi, S.; Takahashi, T.; Suzuki, K. I.; Kawamura, S.; Satoh, M.; Chiba, Y.; Orikasa, S. *Urology* **1999**, *53*, 228–235.
(16) Taton, T. A.; Mirkin, C. A.; Letsinger, R. L. *Science* **2000**, *289*, 1757–1760.
(17) Bernard, P. S.; Wittwer, C. T. *Clin. Chem.* **2002**, *48*, 1178–1185.
(18) Li, H.; Rothberg, L. J. *Anal. Chem.* **2004**, *76*, 5414–5417.
(19) Thompson, D. G.; Enright, A.; Faulds, K.; Smith, W. E.; Graham, D. *Anal. Chem.* **2008**, *80*, 2805–2810.
(20) Chan, W. C.; Nie, S. *Science* **1998**, *281*, 2016–2018.
(21) Skvortsov, D.; Abdueva, D.; Curtis, C.; Schaub, B.; Tavare, S. *Nucl. Acids. Res.* **2007**, *35*, 4154–4163.
(22) Dudley, A. e. M.; Aach, J.; Steffen, M. A.; Church, G. M. *Proc. Natl. Acad. Sci.* **2002**, *99*, 7554–7559.
(23) Hart, T.; Zhao, A.; Garg, A.; Bolusani, S.; Marcotte, E. M. *PLoS ONE* **2009**, *4*, e7088.
(24) Sanchez, F. G.; Diaz, A. N.; Diaz, A. F. G.; Eremin, S. A. *Anal. Chim. Acta* **1999**, *378*, 219–224.
(25) High, K.; Meng, Y.; Washabaugh, M. W.; Zhao, Q. J. *Anal. Biochem.* **2005**, *347*, 159–161.
(26) Toriello, N. M.; Liu, C. N.; Mathies, R. A. *Anal. Chem.* **2006**, *78*, 7997–8003.
(27) Parks, S. B.; Popovich, B. W.; Press, R. D. *Am. J. Clin. Pathol.* **2001**, *115*, 439–447.
(28) Ma, Z.; Hong, Y.; Zhang, M.; Su, M. *Appl. Phys. Lett.* **2009**, *95*, 233101.
(29) Wang, G.; Harrison, I. R. *Thermochim. Acta* **1994**, *231*, 203–213.
(30) Wu, X.; Qin, W.; He, W. *J. Mol. Catal. A: Chem.* **2007**, *261*, 167–171.
(31) Cohn, J. L.; Uher, C. *J. Appl. Phys.* **1989**, *66*, 2045–2048.
(32) Hill, H. D.; Millstone, J. E.; Banholzer, M. J.; Mirkin, C. A. *ACS Nano* **2009**, *3*, 418–424.